

Mechanism of skull suture maintenance and interdigitation

Takashi Miura,¹ Chad A. Perlyn,² Masato Kinboshi,³ Naomichi Ogihara,⁴ Mikiko Kobayashi-Miura,⁵ Gillian M. Morriss-Kay⁶ and Kohei Shiota⁷

¹Department of Anatomy and Developmental Biology, Kyoto University Graduate School of Medicine, Kyoto, Japan

²Division of Plastic Surgery, Washington University School of Medicine, St. Louis, MO, USA.

³Faculty of Medicine, Kyoto University, Kyoto, Japan

⁴Department of Physical Anthropology, Kyoto University Graduate School of Science, Kyoto, Japan

⁵Institute for Virus Research, Kyoto University, Kyoto, Japan

⁶Department of Physiology, Anatomy and Genetics, Oxford, UK

⁷Department of Anatomy and Developmental Biology and Congenital Anomaly Research Center, Kyoto University Graduate School of Medicine, Kyoto, Japan

Abstract

Skull sutures serve as growth centers whose function involves multiple molecular pathways. During periods of brain growth the sutures remain thin and straight, later developing complex fractal interdigitations that provide interlocking strength. The nature of the relationship between the molecular interactions and suture pattern formation is not understood. Here we show that by classifying the molecules involved into two groups, stabilizing factors and substrate molecules, complex molecular networks can be modeled by a simple two-species reaction–diffusion model that recapitulates all the known behavior of suture pattern formation. This model reproduces the maintenance of thin sutural tissue at early stages, the later modification of the straight suture to form osseous interdigitations, and the formation of fractal structures. Predictions from the model are in good agreement with experimental observations, indicating that the model captures the essential nature of the interdigitation process.

Introduction

The mammalian skull vault consists of five principal bones (the paired frontals and parietals and unpaired interparietal), and adjacent margins of the membranous skull vault bones form the cranial sutures, in which growth of the skull vault occurs. Six primary sutures of the cranial vault exist, including the paired coronal sutures (between the frontal and parietal bones), the paired lambdoid sutures (between the parietal and interparietal bones), the single sagittal suture (between the parietal bones), and the single human metopic or murine posterior frontal suture (between the paired frontal bones). Interdigitations found within the sutures of the cranial vault are of two types. The coronal and sagittal sutures are serrated, with the bone edges having a notched or sawlike appearance. A denticulate pattern also exists, in which small toothlike projections of the articulating bones widen towards their free ends; this is seen in

the lambdoid sutures (Sperber 2001). Each cranial suture is first formed as a thin strip of undifferentiated tissue between two skull bones. It is not until after birth that the linear suture line begins to form a wave pattern (Fig. 2a). In the late stage of growth, a complex interdigitated structure that has a noninteger fractal dimension is sometimes formed (Long, 1985; Masuda & Yohro, 1987; Saito et al. 2002; Lynnerup & Jacobsen, 2003; Yu et al. 2003; Wu et al. 2007).

Many growth and transcription factors are known to be involved in sutural growth (Morriss-Kay & Wilkie, 2005; Rice, 2005; Slater et al. 2008), yet identification of the molecules involved and their interactions has not led to an explanation of the mechanism of suture interdigitation. It has been proposed that, functionally, the interdigitation is related to mechanical tension (Moss, 1961; Jaslow, 1990; Byron et al. 2004), and a model has been proposed to explain the mechanism by which the fractal structure of sutural tissue is generated (Oota et al. 2004). The model utilizes the Eden model, random growth of the interface, to model the formation of the interdigitated structure (Supplementary data 1). However, the model assumes that the ragged edges of bones are formed before the two edges come close, which is very different from the actual dynamics (Fig. 2a). Moreover, this model fails to incorporate known molecular inter-

Correspondence

Takashi Miura, Department of Anatomy and Developmental Biology, Kyoto University Graduate School of Medicine, Yoshida Konoe-cho, Sakyo-Ku, Kyoto 606-8501, Japan. E: miura-takashi@umin.net

Accepted for publication 27 August 2009

Article published online 6 October 2009

actions occurring in the developing suture, making it difficult to integrate the proposed fractal dynamics from the model with experimental evidence obtained from molecular developmental biology studies.

In the present study, we established a simple model that can generate the interdigitated structure based on experimental data, and experimentally verify the model. First, we used human and mouse skull specimens to observe the process of suture interdigitation. Next, we listed the molecules involved in the developmental process, and classified them into three categories depending on localization and function. Then, according to the data we defined two factors, tissue differentiation state (u) and substrate concentration (v), to describe the situation and formulated a simple two-species reaction–diffusion model. We numerically tested the behavior of the model concentrating on the basal effect of substrate molecules (a_0) and verified the model with various experimental methods. The model-based predictions were in good agreement with experimental results, suggesting that the model captures the essential features of the mechanism of skull suture interdigitation.

Materials and methods

Observation of skull specimen and image analysis

The human skull collection was provided by the Kyoto University Museum (Department of Anthropology). The specimens were collected during 1900–1930 in Japan. A complete list of the specimens used is provided in Supplementary data 2. Sagittal sutures were traced using a magic pen and Scotch tape, and the traced patterns were digitized using a flatbed scanner (Epson PM-T960). The traced patterns were skeletonized to avoid errors caused by differences in line thickness.

The suture pattern was skeletonized and the amplitude and fractal dimension were measured using IMAGEJ (Abramoff et al. 2004) and *Mathematica*. The coordinates of skeletonized points (x_i, y_i) were measured using IMAGEJ wand tool and stored in text files. Then the average amplitude of the pattern was calculated as follows. First, we defined a line which represents the center of the points using the least – squares method. Next, we calculated the sum of the distance between (x_i, y_i) and the obtained line. The value is divided by the number of points to obtain the average distance between the center line and the points, which should represent the average amplitude of the measured points. We used the box-count method to obtain fractal dimensions with the IMAGEJ program. The principles of the box-count method are described in Falconer (2003).

Organ cultures of mouse skull

We used ICR mice because they are reasonably homogeneous from a genetic point of view. Skull vaults of 3-week-old ICR mice were dissected with the dura mater and pericranium left *in situ*, and placed on a culture plate with DMEM with 10% fetal bovine serum and antibiotics (GIBCO). The explant was incubated at 37 °C; the culture medium was changed every other day.

Whole mount tartrate-resistant acid phosphatase (TRAP) staining

Skull vaults of 3-week-old ICR mice were dissected and fixed in 4% PFA overnight. After three washes with phosphate-buffered saline (PBS), the skull was immersed in staining solution (100 mM sodium acetate buffer (pH5.0), 50 mM sodium tartrate, 0.1 mg mL⁻¹ sodium naphthol AS-MX phosphate (dissolved in *N,N*-dimethylformamide), 0.6 mg mL⁻¹ fast violet LB, and 0.1% Triton X-100). After the color had developed, the reaction was stopped by washing several times with PBS.

Immunohistochemistry

The skull vaults of 3-week-old ICR mice were fixed overnight in 4% paraformaldehyde (PFA). Then the samples were decalcified in decalcification buffer (10% acetic acid, 4% formaldehyde and 0.85% NaCl), dehydrated and embedded in paraffin. The paraffin block was cut with a microtome (10 μ m), mounted on slides and deparaffinized. The sections were blocked with 1.5% normal goat serum for 1 h at room temperature and treated with primary antibody at 4 °C, overnight. Signals were visualized with the standard protocol using a Vector Elite ABC kit. Primary antibodies used were: FGF2 (Santa Cruz Biotechnology, 1 : 100), FGF18 (Santa Cruz Biotechnology, 1 : 100), and BMP4 (R&D systems, 1 : 100). All the experiments were done with more than three specimens.

Reverse transcription-polymerase chain reaction (RT-PCR)

The dura mater of 3W ICR mouse skulls was dissected and its mRNA was extracted using Sepasol (Nacalai Tesque Inc.). The RNA was analyzed using a one-step RT-PCR kit (RT-PCR High Plus, Toyobo Inc.). The following primers were used:

G3PDH: forward 5'-ACCACAGTCCATGCCATCAC-3', reverse: 5'-TCCACCACCTGTTGCTGTA-3'.

BMP4: forward 5'-CCCGGTCTCAGGTATCA-3', reverse 5'-GAAGGCAAGAGCGCGAGG-3'.

FGF2: forward 5'-AACCGGTACCTTGCTATGAAG-3', reverse 5'-GTTCGTTTCAGTGCCACATAC-3'.

TGF β 1: forward 5'-TACAGGGCTTTCGATTACAGC-3', reverse 5'-CGCACACAGCAGTTCTCTC-3'.

Western blotting

Pericranium and dura mater tissues of a same age were dissected and homogenized in sample buffer (50 mM Tris–HCl pH 6.8, 2% SDS, 6% β -mercaptoethanol, 10% glycerol and 0.01% BPB). After the sample concentration was measured by the Bradford assay, samples were boiled at 70 °C for 15 min and electrophoresed in a 15% polyacrylamide gel. Then they were transferred to a PVDF membrane (Nippon pole) and incubated in a 5% ECL blocking reagent (Amersham) for 1 h. The membrane was incubated in primary antibody at 4 °C overnight. After being washed with TBST for 60 min, they were incubated in 100 000 \times diluted HRP-conjugated secondary antibody for 30 min. After another wash with Tris-buffered saline Tween-20 (TBST) for 30 min, specific protein was visualized with ECL Advance reagent (Amersham).

microCT

ICR mice were anesthetized with Avertin. The anesthetized mouse was held on a styrene foam stand and fixed with Scotch tape. ScanXmate-A808S (Comscantech Co., Ltd.) was used. We used 80 kV and 90 μ A for exposure. The dose of ionizing radiation was about 300 mSv h⁻¹ for each exposure (estimated from manufacturer's data). Total exposure time per observation was around 20 min. The volume data were visualized using AMIRA software (Visage Imaging Inc.). The spatial resolution of the data was around 30 μ m voxel⁻¹. We have obtained the time course of suture development during 3–8 weeks in seven mice. Details of the method will be published separately.

Numerical calculation

All numerical experiments were done using Apple PowerPC G5 with the C++ program (Supporting data 1) with the explicit finite difference scheme. Part of the data was obtained by using the *fles_fft* library (developed by M. Nonomura, D. Ueyama and R. Kobayashi; Department of Mathematical and Life Sciences, Hiroshima University), which calculates a Fitz-Hugh–Nagumo type reaction–diffusion model with a fully implicit scheme. Source codes are available on request. Typical simulation parameters used were: $a_0 = 0.05$, $a_1 = 0.5$, $a_2 = 0.1$, $a_3 = 0.1$, $d = 4.0$,

Results

Change in suture pattern during development

Sutures are straight in the newborn human skull (Fig. 1a), but adult sutures are interdigitated (Fig. 1b). To observe the process of this pattern formation in detail, we chose younger specimens and traced the pattern of sagittal sutures of human skull specimens and measured the amplitude of interdigitation and fractal dimension. The amplitude and fractal dimension of sutural interdigitation increased with age, but the correlation was not strong (Fig. 1c,d). It seems that the process of pattern formation using human specimens could not be observed in detail due to extensive individual variation. Therefore, we used noninvasive microCT to observe the development of mouse sagittal suture interdigitation. We observed the time course of the interdigitation on the surface of the skull (Fig. 1e–f), confirming the observations in human skulls.

Formulation of a mathematical model

To better understand the dynamics of suture line pattern formation within the context of our current understanding of the molecular control of suture development, we have formulated a mathematical model. First, we chose key molecules that are directly involved in osteogenic differentiation in sutural tissue. Then, we classified these key molecules according to their localization and effect (Table 1). Molecules that are expressed in differentiating bone and

promote osteogenesis (Runx2 (Komori et al. 1997; Otto et al. 1997) and Osterix (Nakashima et al. 2002), and molecules that are expressed in mesenchyme and inhibit osteogenesis [Noggin (Warren et al. 2003) and Twist (Bialek et al. (2004))] are defined as stabilizing factors as they make the cell differentiation state bistable via a positive feedback mechanism. We assume some saturation mechanism works to make the tissue infinitely osteogenic, which we think is a natural assumption. This saturation mechanism is implemented as a cubic term in our model. One of the stabilizing factors, Noggin, is a diffusible signaling molecule, and random cell movement could be observed during this process (data not shown), so we include the diffusion term to express the effect of spatial propagation of the differentiation state. Molecules that are expressed in undifferentiated or differentiating mesenchyme but promote osteogenesis [FGF2 (Iseki et al. 1997), FGF18 (Ohbayashi et al. 2002), and BMP4 (Warren et al. 2003)] are defined as substrate molecules. We next defined two variables, u as the tissue differentiation state and v as the substrate molecule concentration. The effect of the stabilizing factors can be incorporated into the variable u , and as a result the tissue differentiation state u has two stable states – bone (+1) and undifferentiated mesenchyme (–1). We then defined the substrate molecules as produced by undifferentiated mesenchymal tissue and promoting osteogenesis (Fig. 2a). The system can then be formulated as a modified form of a Fitz-Hugh–Nagumo type reaction–diffusion model (Ohta et al. 1989; Hagberg & Meron, 1994):

$$u' = u - u^3 + a_1 v + a_0 + \Delta u \quad (1)$$

$$v' = -a_2 u - a_3 v + d \Delta v \quad (2)$$

where a_0 , a_1 , a_2 , a_3 , and d are positive constants (Fig. 2b). a_1 represents the efficacy of the substrate signal to differentiate tissue, and the effect of FGF receptors is included in this term. a_0 represents the basal substrate effect. a_2 and a_3 represent the substrate production rate and substrate decay, respectively. d represents the ratio between the substrate diffusion coefficient and propagation speed of the differentiated state u . Δ represents Laplacian and actual form is $\frac{\partial^2}{\partial x^2}$ in one dimension and $\frac{\partial^2}{\partial x^2} + \frac{\partial^2}{\partial y^2}$ in two dimensions. We set d larger than one to represent the fact that propagation of the differentiated state is slower than molecule diffusion in this case. The behavior of this system has been mathematically analyzed previously (Ohta et al. 1989; Hagberg & Meron, 1994).

The model can reproduce the maintenance of suture thickness

The one-dimensional simulation of this system reproduces the maintenance of thin sutural tissue (Fig. 3). Here we

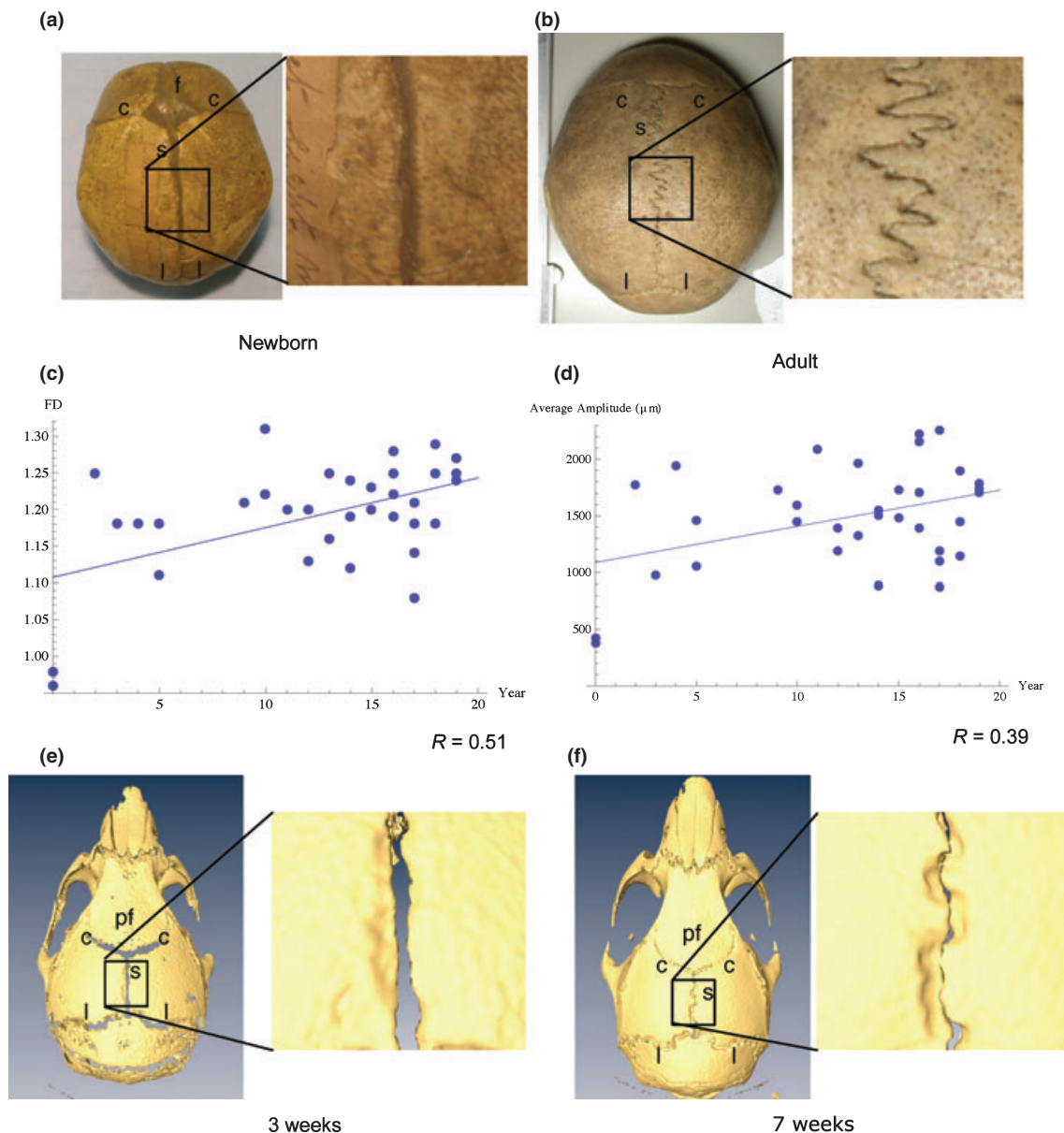


Fig. 1 Development of skull suture interdigitation. (a) In the newborn human skull, the sagittal suture is straight. (b) In the adult human skull, the sagittal suture shows interdigitation. (c) Time course of fractal dimension in the human skull suture. The correlation is moderate according to Cohen's scale (Cohen 1988). (d) Time course of average amplitude change in the human skull suture. The correlation is moderate according to Cohen's scale (Cohen 1988). (e) MicroCT observation of a living mouse skull at 3 weeks. The sagittal suture remains straight. (f) MicroCT observation of the same mouse at 7 weeks. Interdigitation is present. c, coronal suture; s, sagittal suture; l, lambda suture; f, frontal suture; pf, posterior frontal suture.

consider the osteogenic status of a frontal section of sagittal suture (Fig. 3a). When expanded or compressed in the model, the sutural tissue spontaneously returned to its original steady state (Fig. 3b, Supplementary data 3). An intuitive explanation of the mechanism is that as the undifferentiated sutural tissue becomes slightly thicker, there is an increase in undifferentiated mesenchyme and substrate production, which promotes osteogenesis and hence advancement of the osteogenic front. The opposite

process takes place if the undifferentiated sutural tissue becomes slightly thinner. This feedback mechanism maintains the suture thickness in this model.

The model can reproduce suture interdigitation

To demonstrate why the suture interdigitates, we undertook a two-dimensional simulation using the model. Here we considered the two-dimensional domain including a

Table 1 Molecules involved in cranial suture development

Name	Type	Localization	Function	References
Runx2 (Cbfa1)	Transcription factor	Bone	Promotion	Komori et al. (1997), Otto et al. (1997)
Osterix	Transcription factor	Bone	Promotion	Nakashima et al. (2002)
Noggin	Extracellular signaling molecule	Mesenchyme	Inhibition	Warren et al. (2003)
Twist	Transcription factor	Mesenchyme	Inhibition	Bialek et al. (2004)
TGF- β	Extracellular signaling molecule	Mesenchyme	Promotion	Opperman et al. (1997), Mooney et al. (2007)
BMP4	Extracellular signaling molecule	Mesenchyme	Promotion	Warren et al. (2003)
FGF2	Extracellular signaling molecule	Mesenchyme	Promotion	Iseki et al. (1997)
FGF18	Extracellular signaling molecule	Mesenchyme	Promotion	Ohbayashi et al. (2002)
FGFR1	Receptor	Mesenchyme	Promotion	Morriss-Kay & Wilkie (2005)
FGFR2	Receptor	Mesenchyme	Promotion	Morriss-Kay & Wilkie (2005)
FGFR3	Receptor	Mesenchyme	Promotion	Morriss-Kay & Wilkie (2005)
Msx2	Transcription factor	Mesenchyme	Promotion	Kim et al. (1998)
Alx4	Transcription factor	Mesenchyme	Promotion	Rice et al. (2003)
Dlx5	Transcription factor	Mesenchyme	Promotion	Holleville et al. (2003)

suture line (Fig. 4a). We could reproduce the sequence of change from the onset of interdigitation in the undifferentiated region to the formation of a serrated structure while the sutural width remained constant (Fig. 4b, Supplementary data 4). The dynamics was in good agreement with actual skull suture dynamics observed *in vivo* (Fig. 4c). We estimated that the unit of t in this simulation is around 1 h. The mechanism of interdigitation is explained as follows: it is impossible to form a completely straight suture line, so there exist small convexities or concavities in the initial form of the suture line. Then, within a certain parameter range, a slightly protruded bone front should grow faster than other regions as it is surrounded by undifferentiated mesenchyme and hence should be exposed to a higher substrate concentration. The complementary area of slight concavity within the osteogenic front should retreat as it has less mesenchymal tissue around it and therefore should be exposed to a lower substrate concentration. Because of this mechanism, small perturbations of form grow with time, resulting in interdigitation of the sutural tissue.

Sprouting and retraction of the interdigitation pattern

Two predictions come from the above simulation. First, the simulation pattern will on occasion include sprouting of the undifferentiated suture line (Fig. 4b, red circle), which looks unusual at first. However, such "sprouting" patterns are frequently found in human skull specimens (Fig. 4d, red circles), which confirms the prediction.

Another prediction is that bone resorption should occur in the model, as suggested by previous authors (Rice et al. 1997; Byron, 2006). To test whether the process of bone resorption can occur in sutural tissue, we undertook an organ culture experiment. During the first 7 days of culture, the developing skull tissue within the suture showed small sites of tissue retraction (Fig. 5a, b), indicating that the pre-

dicted bone resorption does occur in interdigitating sutural tissue. Furthermore, in this culture system, growth of the tissue explant was not observed, suggesting that the interdigitation process proceeds independently of brain growth and associated calvarial expansion. The existence of osteoclastic activity in this tissue is supported by the TRAP stain (Fig. 5c) or MMP9 immunoreactivity (Fig. 5d). An analysis of mouse skull suture development *in vivo* confirmed that the osteogenic front retracts at the site of interdigitation (Fig. 5e-j). We also observed a quite complex overhung pattern in the human skull (Fig. 8a) which cannot be generated without retraction of the osteogenic front.

Differences in interdigitation between the superficial and deep surface result from localized substrate production

We further tested whether the model can predict what occurs when the degree of interdigitation varies. One well-known example is the pattern difference between the surface and deep areas of the skull: suture lines deeper in the skull are thinner, have less interdigitation, and are occasionally fused (Fig. 6a). If we increase the basal activity of the substrate, i.e. increase a_0 , instability is less likely to occur because the effect of the substrate molecule is saturated. If we make a_0 too large, the suture line fuses as the stabilizer can no longer keep the undifferentiated tissue stable (Fig. 6b). We hypothesized that the difference stemmed from the fact that a substrate molecule is provided from the deeper side of the skull, i.e. from the dura mater (Fig. 6c) as the dura mater influences suture patency (Gagan et al. 2007). We confirmed this prediction from the model using immunohistochemistry and Western blotting to demonstrate that one of the substrate molecules is indeed produced more in the dura mater than in the pericranium (Fig. 6d-f).

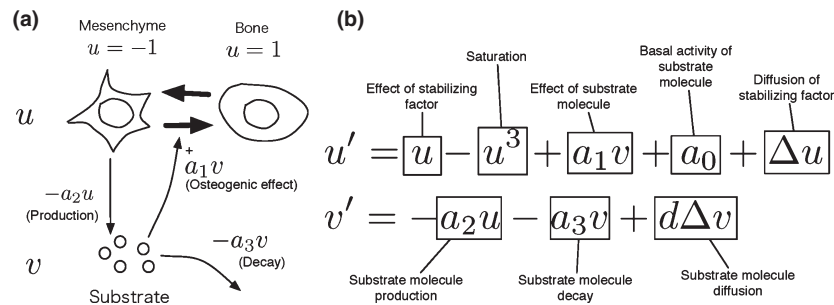


Fig. 2 (a) The model scheme. We included two factors, osteogenic differentiation state of a tissue (u) and substrate concentration (v). Mesenchyme ($u = -1$) and bone ($u = 1$) are two stable states and do not interchange easily. Mesenchymal cells produce substrate molecules which promote the differentiation of undifferentiated mesenchyme. (b) Governing equations of the system and explanations of each term.

Interdigitation and fusion of the posterior frontal suture result from increased substrate production

The murine posterior frontal suture (frontal suture in humans) fuses at later stages. We used microCT to observe the time course of this procedure in a single specimen (Fig. 7a). We observed that at 7 weeks, the originally patent posterior frontal suture became fused, while the sagittal suture remained patent. The posterior frontal suture becomes thick whereas the sagittal suture remains more or less the same, indicating that osteogenic activity is stronger in the posterior frontal suture area.

It has been speculated that the difference is due to some diffusible factor like transforming growth factor beta (TGF β) or FGF2 from the underlying dura mater (Fig. 7b, Bradley et al. (1999); Spector et al. (2000); Kwan et al. (2008)). To confirm whether our model reproduces this phenomenon, we undertook a numerical simulation with a low and high external supply of substrate molecule. The pattern disappears if the substrate supply is sufficiently high (Fig. 7c). The intuitive explanation is as follows: if the concentration of substrate is too high, the stabilizing factors cannot keep the region undifferentiated and the entire region becomes bone. To confirm the previous reports we isolated mRNA from the dura mater underlying sagittal and posterior frontal sutures and observed the gene expression pattern of substrate molecules. mRNA levels of the substrates were high in the dura mater of the posterior frontal region, indicating that the posterior frontal suture fuses because of the strong substrate signal from the dura mater.

Formation of the fractal structure results from a gradual change of parameters

In the late stage of growth, we observed a very complex self-similar fractal pattern that consists essentially of one continuous line (Fig. 8a). However, when we ran the simulation longer to reproduce this pattern, a labyrinthine pattern developed (Fig. 8b), which appears quite different from the actual pattern noted. Functionally, the labyrinthine pattern

is not very useful because the sprouting is basically formed as junctions within a single bone and does not increase interlocking strength. Therefore we sought an additional biological condition that should change the model's behavior. As the thickness of the undifferentiated sutural tissue decreases after birth (Fig. 1a) and its fibrosis occurs at a very late stage (Cohen & MacLean, 2000), we postulated that the diffusion coefficient of the signaling molecules in general decreases with time. We introduced this factor by multiplying the diffusion coefficients of u and v by $h(t)$, which is an exponentially decreasing function of t (Fig. 8c). The simulation result became one continuous line which resembles the actual observed pattern (Fig. 8d), and we detected a fractal dimension larger than $D = 1.6$ in this pattern. The intuitive explanation is as follows: in the original model, the fastest growing wavenumber component becomes unstable and a pattern with a characteristic wavelength is formed out of a nearly straight line (Ohta et al. 1989). Running the simulation too long results in sprouting. However, with the time-dependent diffusion coefficient parameter, the fastest growing wavenumber increases with time. As a result, after a certain time, pattern formation occurs on a smaller scale – part of the previously formed pattern becomes unstable and a larger wavenumber component is added to the original pattern (Fig. 8e). This is similar to carrying out the simulation for a short time again and again with a different spatial scale. This is analogous to generation of the Koch curve (Long, 1985; Masuda & Yohro, 1987: supplementary data 5), which should result in the formation of a fractal structure.

Discussion

Relationship between different classes of models

In both an experimental and theoretical sense there are several classes of models, and each model has its own role. For example, when considering the differentiation of a tissue from an experimental point of view, we sometimes use a

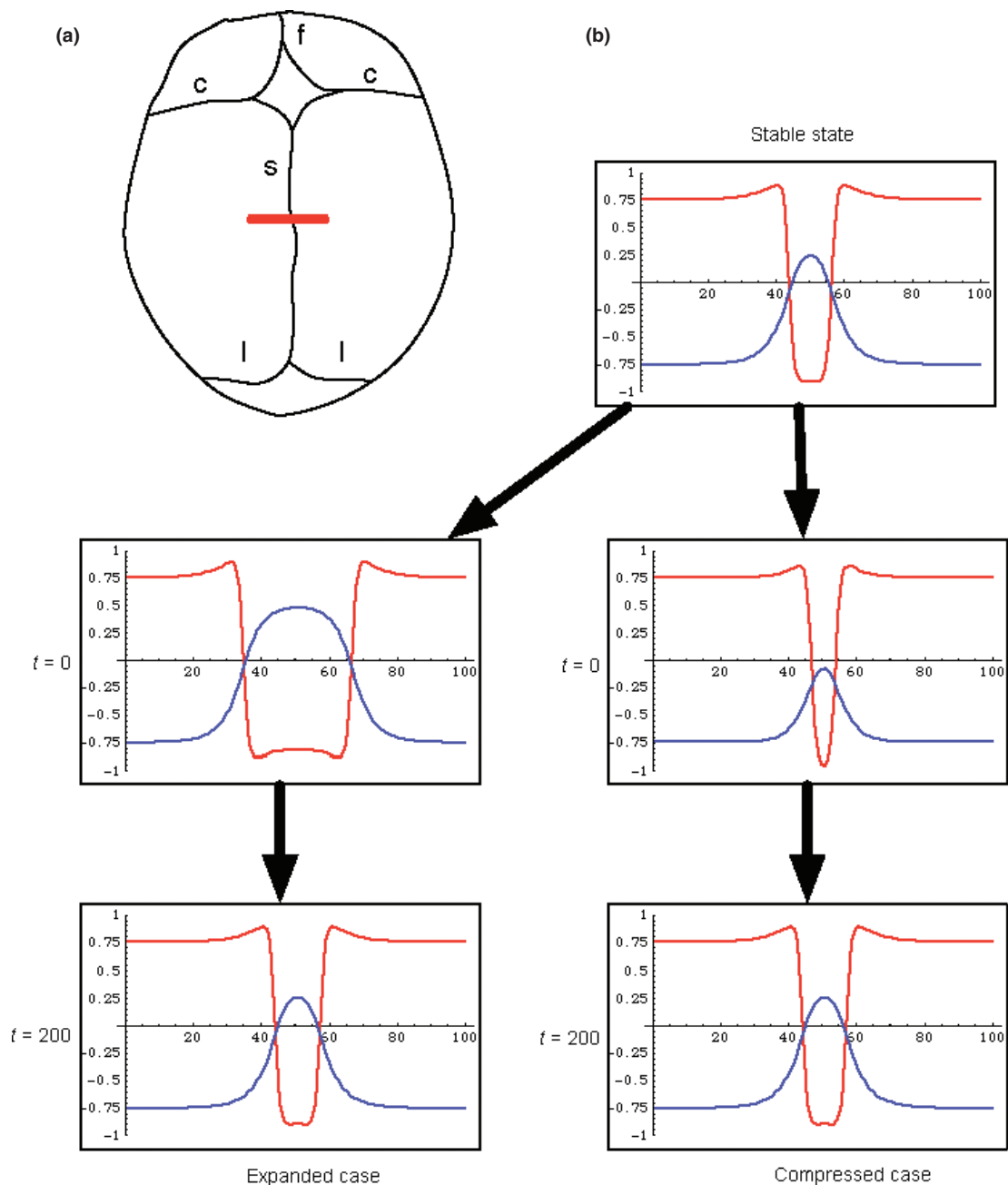


Fig. 3 The model reproduces suture width maintenance. (a) Scheme of the human skull at birth. The suture maintenance simulation region is depicted as a red line. (b) One-dimensional simulation showed the maintenance of thin sutural tissue. The red line represents u and blue line represents v . When the sutural tissue width was changed, substrate production was changed accordingly, which resulted in the maintenance of constant tissue thickness (see text). Simulation parameters: $a_0 = 0.05$, $a_1 = 0.5$, $a_2 = 0.1$, $a_3 = 0.1$, $d = 4.0$. The unit of x -axis is $50 \mu\text{m}$. c, coronal suture; s, sagittal suture; l, lambdoid suture; f, frontal suture.

simplified scheme like the balance between “cell proliferation” and “differentiation”, which neglects some molecular details but is very useful for understanding the overall behavior of the system. We also use a detailed molecular interaction scheme to understand the phenomena, but the situation is much better when we have a simpler view as previously described. In physics the terms “toy model” and

“full model” are used to distinguish these models. Toy models lack details but provide a clear view of the overall behavior of the system, while full models contain detailed information of the system but sometimes end up with a mere reproduction of the phenomena by computation. It depends on the situation which comes first. In some cases, a toy model was discovered first heuristically, and in other

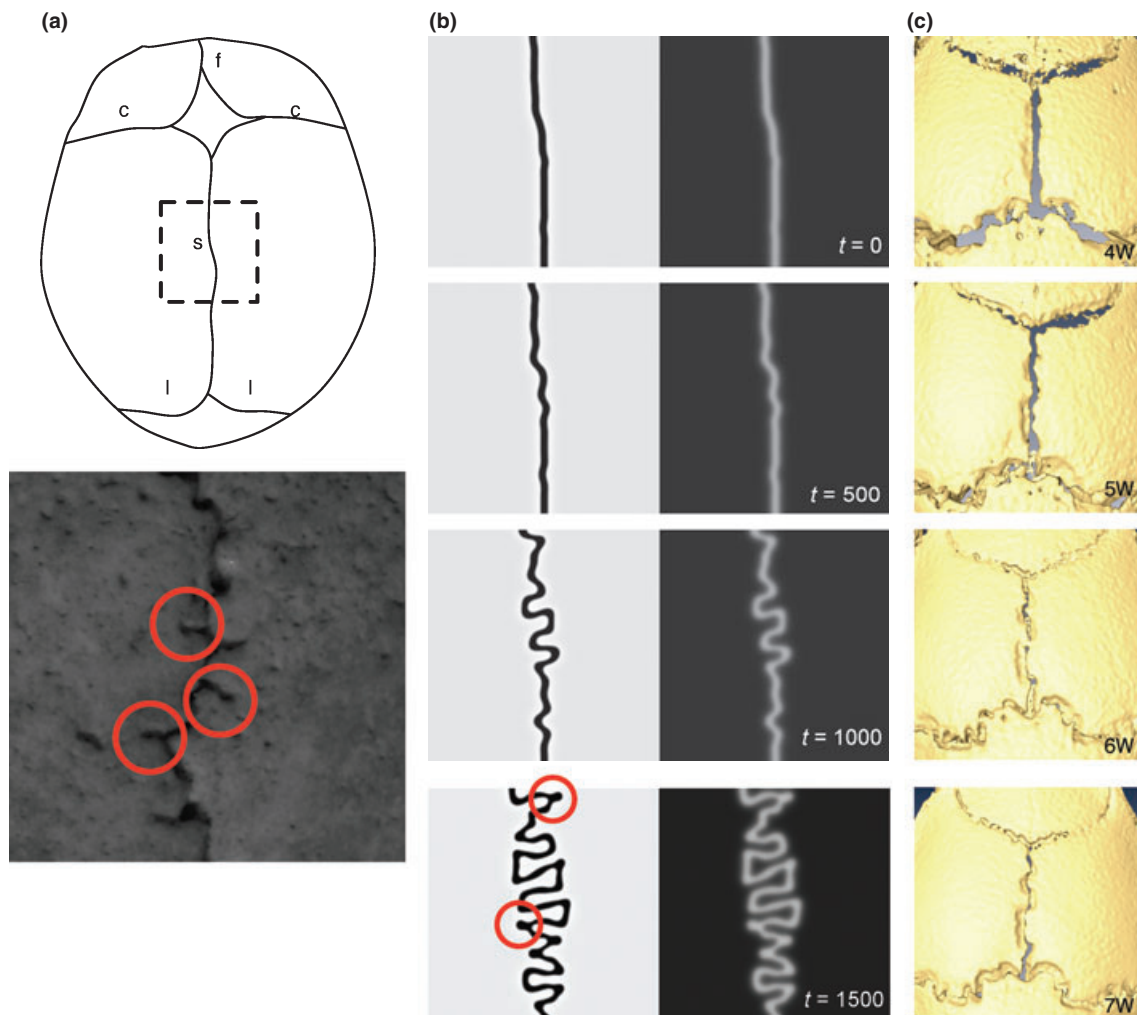


Fig. 4 The model reproduces suture interdigitation. (a) Scheme of the human skull at birth. The interdigitation simulation region is depicted by a dashed box. (b) Two-dimensional simulation of the model with a straight line initial condition faithfully mimicked the pattern formation of a suture line. The white area represents a higher value. Sometimes “sprouting” patterns were observed in simulation results (red circle). (c) Actual pattern formation dynamics in the mouse skull from 4 to 7 weeks. The formation of interdigitation resembles results of simulation. (d) Actual pattern in a human skull specimen. The sprouting pattern was also found in actual specimens (red circle). Simulation parameters: $a_0 = 0.05$, $a_1 = 0.5$, $a_2 = 0.1$, $a_3 = 0.1$, $d = 4.0$. The width and height of the simulation area roughly corresponds to 1 cm. c, coronal suture; s, sagittal suture; l, lambda suture; f, frontal suture.

cases, a full model came first and then a simpler model was derived by approximation. For example, in the case of limb development, the very first model was heuristic (Newman & Frisch, 1979), followed by a detailed description of a full model (Hentschel et al. 2004). The full model was recently reduced to a simplified one somewhat different from the original using a number of mathematical techniques and explicit biological assumptions (Alber et al. 2008).

The model formulated here is a “toy model” according to the previous classification. Also somewhat abstract, this model can be related to known molecular interactions and can be directly tested experimentally. We used a conventional classification to simplify the model, so that it is accessible to both mathematicians and developmental

biologists. For example, from a mathematical point of view, the model itself is simple enough (two-species reaction–diffusion model) to enable mathematical analysis (Ohta et al. 1989; Hagberg & Meron, 1994). From an experimental point of view, the model uses concepts familiar to developmental biologists (tissue differentiation state and morphogen) to clarify the mechanism, and the effect of genetic modification is easily incorporated, as we showed in the main text. For example, the effect of constitutively active FGFR2 can be assayed by increasing a_0 , which should cause premature fusion or less interdigitation. Such a phenotype is actually observed in Crouzon model mice (Eswarakumar et al. 2004; Perlyn et al. 2006; Olafsdottir et al. 2007).

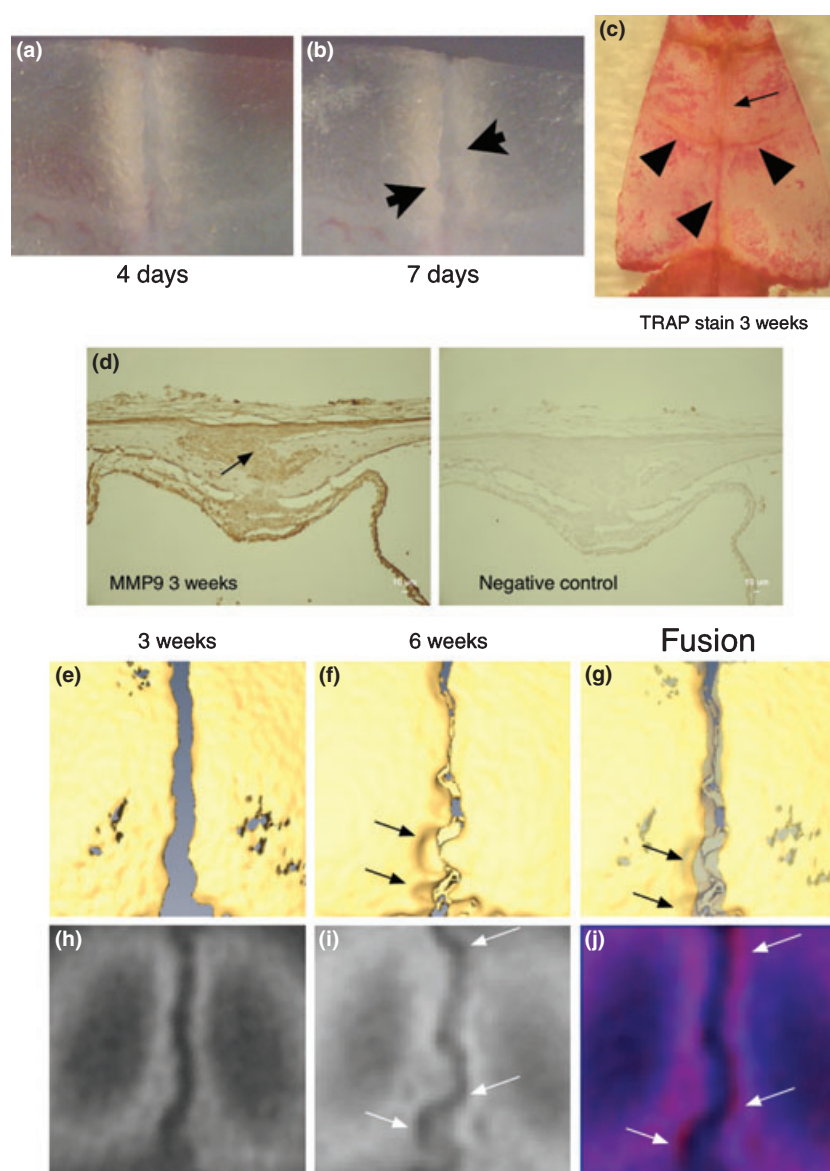


Fig. 5 Retraction of osteogenic front occurs during suture development. (a) Cultured skull specimen after 4 days. (b) Cultured skull specimen after 7 days. Compared with (a), some parts of the osteogenic front have retracted (arrowheads). (c) TRAP staining of a mouse skull (3 weeks old). Staining was detected in suture lines which undergo active interdigitation. (d) Osteoclast activity was also detected in the suture by MMP9 immunohistochemistry (arrow). (e–j) The time course of the development of sutural tissue in a single specimen. (e–g) represents a surface-rendering view and (h–j) shows the observation of a specific section. The suture line was relatively straight at 3 weeks (e,h) but formed interdigitation at 6 weeks (f,i). Superimposition of (e–f) and (h–i) revealed that the suture line retracted in the interdigitating region (arrows in g, j). In (j), plate (h) in red and plate (i) in blue are superimposed. Therefore, red regions are sites of retraction (arrows).

Sprouting pattern

We frequently observed a sprouting pattern both in the simulation and in actual biological specimens, which provides insight into the relationship between the structure and function of the skull suture. It has been hypothesized that the interdigitation of skull sutures functions to strengthen the connections between the skull bones by increasing the surface area of connections. For example, transgenic mice with a larger muscle mass have more inter-

digitated sutures (Byron et al. 2004). Jaslow (1990) undertook fracture tests using goat skull specimens and found that the interdigitation makes the junctions more elastic, which may be beneficial because they can absorb shock. However, the sprouting pattern is a junction inside a single bone and can not be explained from a functional point of view. Schiwy-Bochat (2001) reported that there is a sprouting-only area in the supranasal region. We can produce a sprouting-only pattern with our model (data not shown), and it would be intriguing to predict the change in gene

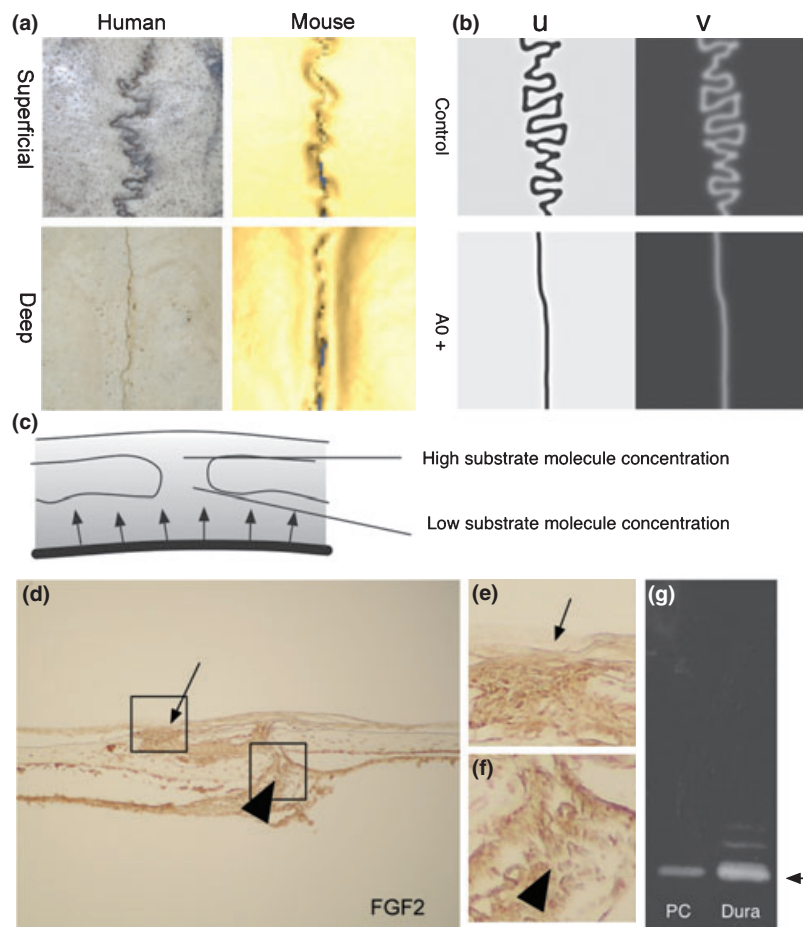


Fig. 6 (a) Difference of sutural interdigitation between the superficial and deep surfaces of the skull. Mouse skull data were obtained using microCT. In both humans and mice, the suture line is thinner and interdigitation is less prominent on the deeper side of the skull. (b) Effect of substrate basal activity a_0 . When a_0 was increased, undifferentiated sutural tissue became thinner and interdigitation less prominent. (c) Working hypothesis of the difference. If there is a source of substrate on the deeper side of the skull, the basal effect of the substrate is stronger on the deeper side, resulting in the observed morphological difference. (d–f) Immunohistochemical localization of substrate molecules in 3-week-old sagittal sutural tissue. Distribution of substrate molecules showed that they were mainly produced in the dura mater, confirming the prediction. In all the specimens tested, we observed stronger staining in the dura mater (arrowheads) than in the pericranium (arrows). Simulation parameters: $a_0 = 0.05$ – 0.1 , $a_1 = 0.5$, $a_2 = 0.1$, $a_3 = 0.1$, $d = 4.0$.

expression by comparing the model parameters and actual patterns.

Formation of the fractal structure

A fractal structure is defined as a pattern which has self similarity – if we magnify part of a fractal structure, a similar pattern appears in a smaller spatial scale (for review, see Falconer, 2003; Mandelbrot, 1983). Theoretically, the way in which a fractal structure is generated is a very interesting problem, as it is known that the reaction–diffusion model does not usually generate a fractal structure (an exception was reported by Hayase & Ohta (2000)). It has been reported that interdigitation has a noninteger fractal dimension in the human skull (Long 1985). The sutural pattern has been frequently compared with a Koch curve (Supplementary data 4), a typical fractal structure, but the

relationship has not been understood. In our model, a time-dependent parameter makes the system behave similarly to the way a Koch curve is generated. Currently, we do not have direct experimental support for this hypothetical mechanism. Time-course observations of a human skull are not available because of x-ray exposure problems, so some experimental verification of the model by time-course observations of larger animals is necessary (Sun et al. 2007). If such time-course data is available, an analysis of spatial frequency data (Wu et al. 2007) can be directly correlated to the model parameters.

Relationship with craniosynostosis

Craniosynostosis, premature fusion of skull bones, can be analyzed using a one-dimensional version of this model and should be useful in elucidating the pathogenesis of this

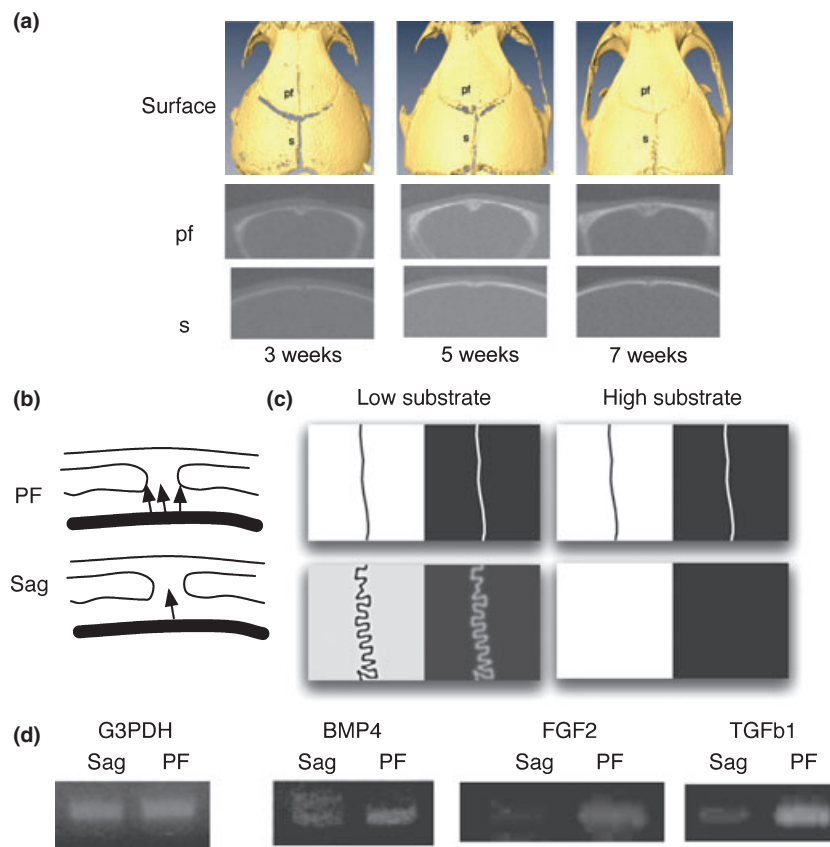


Fig. 7 (a) Time course of posterior frontal suture closure. The surface view and frontal section of a single mouse skull specimen are presented. The posterior frontal (PF) suture was closed while the sagittal suture remained patent at 7 weeks. The posterior frontal suture did not undergo interdigitation. Frontal bones were in general thicker than parietal bones, and edges of the frontal bones became thicker with age. (b) Working hypothesis. The amount of substrate from the dura mater is greater in the posterior frontal suture than in the sagittal suture. (c) Numerical simulation of the model with very high substrate basal activity (a_0). If we increased a_0 too much, the sutural tissue disappeared, mimicking craniosynostosis. (d) Production of substrate molecules in the dura mater. mRNA levels of G3PDH (positive control), BMP4, FGF2 and TGFb1 were compared in the dura mater underlying the sagittal and posterior frontal sutures. Stronger expression of substrate molecules was observed in the posterior frontal region, indicating that the amount of substrate from the dura mater determines the sagittal-posterior frontal difference. Simulation parameters: $a_1 = 0.5$, $a_2 = 0.1$, $a_3 = 0.1$, $d = 4.0$. c, coronal suture; s, sagittal suture; l, lambda suture; pf, posterior frontal suture.

state. Premature fusion of the skull bones causes clinical problems because it prevents the normal expansion of the skull that is required to accommodate the growing brain (Cohen & MacLean, 2000; Morriss-Kay & Wilkie, 2005). This disorder is a relatively common birth defect (1: 2000–3000), and many genetic mutations have been found in those affected (Coster et al. 2007). Our model is simple enough to be analyzed mathematically, and we can derive a strong working hypothesis from it which sheds light on how the suture tissue is maintained and under what conditions the suture closes prematurely.

Hypothesis to test

The model could be extended to incorporate other factors such as cell lineage and tissue growth, which are known to be involved in the process. For example, Jiang et al. (2002) have shown that the frontal and parietal bones have dis-

tinct cell lineages. Lana-Elola et al. (2007) showed that cells in the middle of sutural tissue remain undifferentiated, whereas cells near the edge of the growing osteogenic front become part of the membranous bone. The reaction–diffusion model concentrates on the state of differentiation in a specific location and does not include information on cell fate. An extension of the model may be required to incorporate dynamic cell movement during suture development.

The model presented here may have some relationship with other skeletal structures. For example, there are several models which utilize reaction–diffusion equations to model the formation of bone spicules (Tezuka et al. 2005). We observed the formation of the lumen inside the thickened parietal bone in 3-week old mice, and found that a periodic structure of similar size to sutural interdigitation is formed within the thickness of the bone. The periodic aspect of limb skeletal elements has also been modeled using a reac-

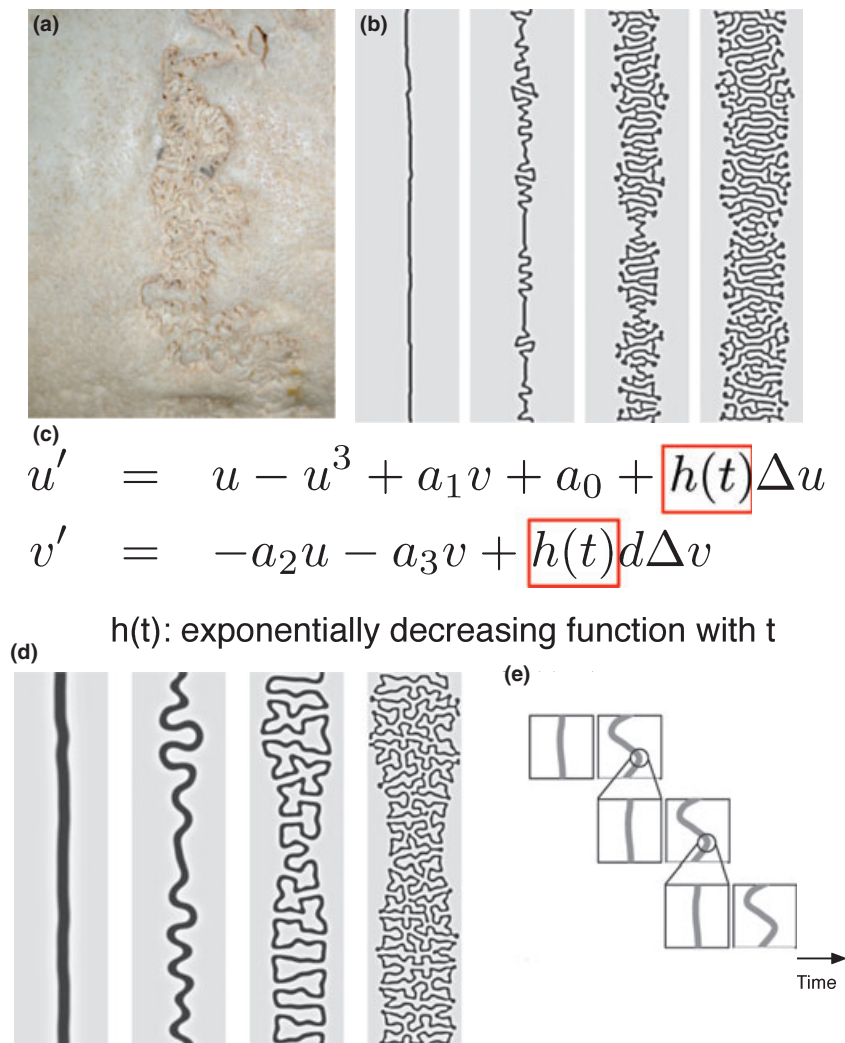


Fig. 8 Formation of a fractal structure in the model. (a) Lambdoid suture of a human skull showed quite a complex fractal pattern. (b) Simulation result of original model, which ended up "labyrinthine" and looked different from the *in vivo* pattern. (c) Modified form of the model. We introduced a time-dependent parameter in the diffusion coefficient to implement fibrosis of the sutural tissue (Cohen & MacLean 2000). (d) Simulation result of the modified model. The pattern became one continuous line, which looked similar to the *in vivo* pattern. (e) Intuitive explanation of the pattern difference. In the modified model, the generated pattern becomes gradually smaller with time, and detailed structure is added onto the original pattern. This procedure is analogous to the formation of a Koch curve, which results in the formation of a fractal structure. Simulation parameters: $a_0 = 0.05$, $a_1 = 0.5$, $a_2 = 0.1$, $a_3 = 0.1$, $d = 4.0$.

tion–diffusion scheme (Newman & Frisch, 1979; Miura & Shiota, 2000). The formation of a periodic structure might be a common feature of many skeletal components.

The relationship with mechanical force can be studied via molecular pathways using our model. It has long been asserted that mechanical force exerts effects on skull suture interdigitation (Byron et al. 2004). Our study suggests that mechanical force is not the only factor that determines suture interdigitation. For example, we observed the onset of interdigitation in an organ culture system in which no external force was applied (Fig. 5a,b). There are several reports in which the expression of a given gene has been changed by exerting mechanical force on the sutural tissue (Fong et al. 2003; Collins et al. 2005; Tholpady et al. 2007;

Jacob et al. 2007). With the model presented here, it is possible to use such experimental results to show how the mechanical load leads to a more interdigitated pattern from a molecular point of view. These data might bridge the gap between molecular function and the anatomical pattern generated by our model.

Acknowledgements

The authors thank Mitsugu Matsushita, Ryo Kobayashi, Daishin Ueyama, Yasuaki Hiraoka, Toshiyuki Nakagaki, Masayasu Mimura, Yasumasa Nishiura, Shigeru Kondo, and Atsushi Mochizuki for helpful discussions and comments, Naoki Morimoto and Shigehito Yamada for image processing and Makoto Nakatsukasa

and Masaharu Motokawa for providing human skull specimens. This work is supported by the Japanese Society for the Promotion of Science.

Author contributions

Takashi Miura designed the whole project and undertook numerical simulation, organ culture, immunohistochemistry and RT-PCR experiments. Chad Perlyn provided mouse skull CT data. Masato Kinboshi and Naomichi Ogihara were involved in microCT data acquisition. Mikiko Kobayashi-Miura undertook image processing of human skull data. Gillian M. Morriss-Kay and Kohei Shiota were involved in critical revision of the manuscript and for provision of laboratory facilities for the initial phase of the work.

References

- Abramoff M, Magelhaes P, Ram S (2004) IMAGEJ processing with IMAGEJ. *Biophotonics Int* **11**, 36–42.
- Alber M, Glimm T, Hentschel HGE et al. (2008) The morphostatic limit for a model of skeletal pattern formation in the vertebrate limb. *Bull Math Biol* **70**, 460–483.
- Bialek P, Kern B, Yang X et al. (2004) A twist code determines the onset of osteoblast differentiation. *Dev Cell* **6**, 423–435.
- Bradley J, Han V, Roth D et al. (1999) Increased IGF-I and IGF-II mRNA and IGF-I peptide in fusing rat cranial sutures suggest evidence for a paracrine role of insulin-like growth factors in suture fusion. *Plast Reconstr Surg* **104**, 129–138.
- Byron CD (2006) Role of the osteoclast in cranial suture waveform patterning. *Anat Rec A Discov Mol Cell Evol Biol* **288**, 552–563.
- Byron CD, Borke J, Yu J et al. (2004) Effects of increased muscle mass on mouse sagittal suture morphology and mechanics. *Anat Rec A Discov Mol Cell Evol Biol* **279**, 676–684.
- Cohen J (1988) *Statistical Power Analysis for the Behavioral Sciences*, 2nd edn. Philadelphia: Lawrence Erlbaum Assoc. Inc.
- Cohen M, MacLean R eds (2000) *Craniosynostosis: Diagnosis, Evaluation and Management*. 2nd edn New York: Oxford University Press.
- Collins JM, Ramamoorthy K, Silveira AD et al. (2005) Expression of matrix metalloproteinase genes in the rat intramembranous bone during postnatal growth and upon mechanical stresses. *J Biomech* **38**, 485–492.
- Coster PJD, Mortier G, Marks LA et al. (2007) Cranial suture biology and dental development: genetic and clinical perspectives. *J Oral Pathol Med* **36**, 447–455.
- Eswarakumar VP, Horowitz MC, Locklin R et al. (2004) A gain-of-function mutation of Fgfr2c demonstrates the roles of this receptor variant in osteogenesis. *Proc Natl Acad Sci USA* **101**, 12555–12560.
- Falconer K (2003) *Fractal Geometry*. New York: Wiley & Sons Inc.
- Fong KD, Nacamuli RP, Lobo EG et al. (2003) Equibiaxial tensile strain affects calvarial osteoblast biology. *J Craniofac Surg* **14**, 348–355.
- Gagan JR, Tholpady SS, Ogle RC (2007) Cellular dynamics and tissue interactions of the dura mater during head development. *Birth Defects Res C Embryo Today* **81**, 297–304.
- Hagberg A, Meron E (1994) From labyrinthine patterns to spiral turbulence. *Phys Rev Lett* **72**, 2494–2497.
- Hayase Y & Ohta T (2000) Self-replicating pulses and Sierpinski gaskets in excitable media. *Phys Rev E* **62**(5 Pt A), 5998–6003.
- Hentschel HGE, Glimm T, Glazier JA et al. (2004) Dynamical mechanisms for skeletal pattern formation in the vertebrate limb. *Proc Biol Sci* **271**, 1713–1722.
- Holleville N, Quilhac A, Bontoux M et al. (2003) BMP signals regulate Dlx5 during early avian skull development. *Dev Biol* **257**, 177–189.
- Iseki S, Wilkie A, Heath J et al. (1997) Fgfr2 and osteopontin domains in the developing skull vault are mutually exclusive and can be altered by locally applied FGF2. *Development* **124**, 3375–3384.
- Jacob S, Wu C, Freeman TA et al. (2007) Expression of Indian hedgehog, bmp-4 and noggin in craniosynostosis induced by fetal constraint. *Ann Plast Surg* **58**, 215–221.
- Jaslow CR (1990) Mechanical properties of cranial sutures. *J Biomech* **23**, 313–321.
- Jiang X, Iseki S, Maxson RE et al. (2002) Tissue origins and interactions in the mammalian skull vault. *Dev Biol* **241**, 106–116.
- Kim HJ, Rice DP, Kettunen PJ et al. (1998) FGF- BMP- and Shh-mediated signalling pathways in the regulation of cranial suture morphogenesis and calvarial bone development. *Development* **125**, 1241–1251.
- Komori T, Yagi H, Nomura S et al. (1997) Targeted disruption of Cbfa1 results in a complete lack of bone formation owing to maturational arrest of osteoblasts. *Cell* **89**, 755–764.
- Kwan MD, Wan DC, Wang Z et al. (2008) Microarray analysis of the role of regional dura mater in cranial suture fate. *Plast Reconstr Surg* **122**, 389–399.
- Lana-Elola E, Rice R, Grigoriadis AE et al. (2007) Cell fate specification during calvarial bone and suture development. *Dev Biol* **311**, 335–346.
- Long CA (1985) Intricate sutures as fractal curves. *J Morphol* **185**, 285–295.
- Lynnerup N, Jacobsen JCB (2003) Brief communication: age and fractal dimensions of human sagittal and coronal sutures. *Am J Phys Anthropol* **121**, 332–336.
- Mandelbrot BB (1983) *The Fractal Geometry of Nature*. New York: Freeman.
- Masuda Y, Yohro T (1987) Are there any regularities in cranial sutures? *Okajimas Folia Anat Jpn* **64**, 39–46.
- Miura T, Shiota K (2000) Tgf beta2 acts as an “activator” molecule in reaction–diffusion model and is involved in cell sorting phenomenon in mouse limb micromass culture. *Dev Dyn* **217**, 241–249.
- Mooney MP, Losken HW, Moursi AM et al. (2007) Anti-tgf-beta2 antibody therapy inhibits postoperative resynostosis in craniosynostotic rabbits. *Plast Reconstr Surg* **119**, 1200–12; discussion 1213–1215.
- Moss M. L. (1961) Extrinsic determination of sutural area morphology in the rat calvaria. *Acta Anat (Basel)* **44**, 263–272.
- Morriss-Kay GM, Wilkie AOM (2005) Growth of the normal skull vault and its alteration in craniosynostosis: insights from human genetics and experimental studies. *J Anat* **207**, 637–653.
- Nakashima K, Zhou X, Kunkel G et al. (2002) The novel zinc finger-containing transcription factor osterix is required for osteoblast differentiation and bone formation. *Cell* **108**, 17–29.
- Newman SA, Frisch HL (1979) Dynamics of skeletal pattern formation in developing chick limb. *Science* **205**, 662–668.

- Ohbayashi N, Shibayama M, Kurotaki Y et al. (2002) FGF18 is required for normal cell proliferation and differentiation during osteogenesis and chondrogenesis. *Genes Dev* **16**, 870–879.
- Ohta T, Mimura M, Kobayashi R (1989) Higher-dimensional localized patterns in excitable media. *Physica D* **34**, 115–144.
- Olafsdottir H, Darvann TA, Hermann NV et al. (2007) Computational mouse atlases and their application to automatic assessment of craniofacial dysmorphology caused by the crouzon mutation *fgfr2(c342y)*. *J Anat* **211**, 37–52.
- Oota Y, Nagamine T, Ono K et al. (2004) A two-dimensional model for sagittal suture of cranium. *Forma* **19**, 197–205.
- Opperman L, Nolen A, Ogle R (1997) TGF-beta 1, TGF-beta 2 and TGF-beta 3 exhibit distinct patterns of expression during cranial suture formation and obliteration *in vivo* and *in vitro*. *J Bone Miner Res* **12**, 301–310.
- Otto F, Thornell AP, Crompton T et al. (1997) *Cbfa1*, a candidate gene for cleidocranial dysplasia syndrome, is essential for osteoblast differentiation and bone development. *Cell* **89**, 765–771.
- Perlyn CA, DeLeon VB, Babbs C et al. (2006) The craniofacial phenotype of the crouzon mouse: analysis of a model for syndromic craniosynostosis using three-dimensional microCT. *Cleft Palate Craniofac J* **43**, 740–748.
- Rice D, Kim H, Thesleff I (1997) Detection of gelatinase B expression reveals osteoclastic bone resorption as a feature of early calvarial bone development. *Bone* **21**, 479–486.
- Rice DPC (2005) Craniofacial anomalies: from development to molecular pathogenesis. *Curr Mol Med* **5**, 699–722.
- Rice R, Rice DPC, Olsen BR et al. (2003) Progression of calvarial bone development requires *foxc1* regulation of *msx2* and *alx4*. *Dev Biol* **262**, 75–87.
- Saito K, Shimizu Y, Ooya K (2002) Age-related morphological changes in squamous and parietomastoid sutures of human cranium. *Cells Tissues Organs* **170**, 266–273.
- Schiwy-Bochat KH (2001) The roughness of the supranasal region – a morphological sex trait. *Forensic Sci Int* **117**, 7–13.
- Slater BJ, Lenton KA, Kwan MD et al. (2008) Cranial sutures: a brief review. *Plast Reconstr Surg* **121**, 170e–178e.
- Spector J, Mehrara B, Greenwald J et al. (2000) A molecular analysis of the isolated rat posterior frontal and sagittal sutures: differences in gene expression. *Plast Reconstr Surg* **106**, 852–861; discussion 862–867.
- Sperber G (2001) *Craniofacial Development*. London: BD Decker, Inc.
- Sun Z, Lee E, Herring SW (2007) Cell proliferation and osteogenic differentiation of growing pig cranial sutures. *J Anat* **211**, 280–289.
- Tezuka K, Wada Y, Takahashi A et al. (2005) Computer-simulated bone architecture in a simple bone-remodeling model based on a reaction–diffusion system. *J Bone Miner Metab* **23**, 1–7.
- Tholpady SS, Freyman TF, Chachra D et al. (2007) Tensional forces influence gene expression and sutural state of rat calvariae *in vitro*. *Plast Reconstr Surg* **120**, 601–611; discussion 612–613.
- Warren S, Brunet L, Harland R et al. (2003) The BMP antagonist *noggin* regulates cranial suture fusion. *Nature* **422**, 625–629.
- Wu Y-D, Chien C-H, Chao YJ et al. (2007) Fourier analysis of human sagittal sutures. *Cleft Palate Craniofac J* **44**, 482–493.
- Yu JC, Wright RL, Williamson MA et al. (2003) A fractal analysis of human cranial sutures. *Cleft Palate Craniofac J* **40**, 409–415.

Supporting Information

Additional Supporting Information may be found in the online version of this article:

Data S1. Mathematica file for Eden collision model.

Data S2. Table of human skull sample in Kyoto university.

Data S3. Mathematica file for suture model (1D).

Data S4. Mathematica file for suture model (2D).

Data S5. Mathematica file for Koch curve generation.

As a service to our authors and readers, this journal provides supporting information supplied by the authors. Such materials are peer-reviewed and may be re-organized for online delivery, but are not copy-edited or typeset. Technical support issues arising from supporting information (other than missing files) should be addressed to the authors.